Applied Catalysis A, General 542 (2017) 350–358

Contents lists available at ScienceDirect

Applied Catalysis A, General

journal homepage: www.elsevier.com/locate/apcata

Feature Article

Solvent-free "green" amidation of stearic acid for synthesis of biologically active alkylamides over iron supported heterogeneous catalysts

Päivi Mäki-Arvela[a], Jeanne Zhu[a], Narendra Kumar[a], Kari Eränen[a], Atte Aho[a], Johan Linden[a], Jarno Salonen[b], Markus Peurla[b], Anton Mazur[c], Vladimir Matveev[c], Dmitry Yu. Murzin[a,*]

[a] Åbo Akademi University, Turku/Åbo, Finland
[b] University of Turku, Turku, Finland
[c] St. Petersburg State University, Russia

ARTICLE INFO

Keywords:
Zeolite
Amidation
Fatty acid

ABSTRACT

Stearoyl ethanolamine was synthesized by amidation of stearic acid with ethanolamine in solventless conditions. Iron containing heterogeneous catalysts supported on SiO_2, Al_2O_3, Beta (BEA), ZSM-12 (MTW) and Ferrierite (FER) were used in this work. Sn-modified Ferrierite and H-Ferrierite were also studied for comparison. Fe-modified catalysts synthesized using solid state ion-exchange and evaporation impregnation methods, were thoroughly characterized with X-ray powder diffraction, scanning electron microscope, FTIR with pyridine, nitrogen adsorption, energy dispersive X-ray microanalysis and Mössbauer spectroscopy. The highest conversion was obtained with Fe-H-FER-20 at 140 °C in 1 h giving 61% conversion and 98% selectivity towards the desired amide. The catalytic performance in terms of turnover frequency per mole of iron was achieved with the catalyst exhibiting the largest amount of Fe^{3+} species, optimum acidity and a relatively low Brønsted to Lewis acid site ratio.

1. Introduction

Amidation of fatty acids is an important reaction, in which fatty alkanolamines are formed as products. Applications of these products are related not only to surfactants, but also to high value-added pharmaceuticals exhibiting several biological effects, such anti-carcinogenic ones [1] and activity against the Alzheimer disease [2]. The use of heterogeneous catalysts makes the process more industrially benign and cheaper, avoiding cumbersome catalyst separation.

Fatty acid amides are typically synthesized with homogeneous catalysts, for example by reacting a fatty acid ester with an alkanolamine in the presence offatty acid chlorides [3] or using potassium hydroxideas reagents [4], which are not environmentally benign procedures. Utilization of fatty acids is beneficial from the viewpoint of expanding the feedstock base and typically acidic and metal modified zeolites and mesoporous materials were used as catalysts. Direct amidation of fatty acids with alkanolamines has been scarcely investigated over heterogeneous catalysts [5–8]. These reactions were mainly conducted in the presence of solvents. In some cases, supported iron catalysts have been applied in acetic acid amidation [9,10]. This acid underwent amidation with several phenylamine derivatives over iron on activated carbon catalyst. A high excess of acid was used in this reaction operating at the temperature close to the boiling point of acetic acid yielding 96% of amides within 1- 5 h depending on the reactant [9]. In addition acetic acid was also amidated with aniline using Fe-Beta zeolite with Si/Al ratio of 15 at 117 °C with an excess of acetic acid under microwave irradiation giving 52% conversion of stearic acid in 15 min [10]. Furthermore, cheap alumina balls were used for production of *n*-isopropylheptanamide from heptanoic acid and isopropylamine resulting in 95% yield at 140 °C in 3 h [11]. In this work [11] the alumina balls were calcined prior to the experiment facilitating their function as adsorbents during amidation reaction. The reactant was a relatively short carboxylic acid and the drawback with alumina balls is that they cannot be used in autoclave. When Cu-SiO_2, Cu-Al_2O_3 and Cu-TiO_2 catalysts were studied in α-amidation of cyclic ethers [12], it was observed that the reaction was influenced by the support type and copper dispersion. Application of non-conventional, sustainable, eco-friendly and highly efficient process technology for production of various types of amides is of immense importance. Oxidative amidation of alcohols with amines was carried out using heteropolyanion-based ionic liquids under microwave irradiation and solvent free reaction media [13]. Formation of primary, secondary and tertiary alkyl amides was reported with bifunctional catalysts. Direct amidation of carboxylic acids with amines using ultrasonic irradiation was investigated using

* Corresponding author.
E-mail address: dmurzin@abo.fi (D.Y. Murzin).

http://dx.doi.org/10.1016/j.apcata.2017.06.006
Received 10 January 2017; Received in revised form 5 April 2017; Accepted 2 June 2017
Available online 02 June 2017
0926-860X/

solid acid sulfonated graphene oxide [14]. Very high yields of amides under shorter reaction time was reported by the authors when sonochemical amidation of carboxylic acid was applied with a reusable solid acid catalyst.

Besides zeolites *per se*, transition and noble metal modified ones have found applications in several industrial processes in the fields of petrochemistry, oil refining, exhaust gas emission abatement, production of specialty and fine chemicals. In the current study besides SiO_2, Al_2O_3 and TiO_2 supports also, Beta (BEA), Ferrierite (FER), and ZSM-12 (MTW) zeolites were modified with Fe using solid state ion-exchange and evaporation impregnation synthesis methods. Sn modified FER was synthesized using evaporation impregnation method. ZSM-12 (MTW) belongs to high silica zeolite group with unidimensional channel systems, 12 membered rings with pore dimensions 0.57 × 0.61 nm. The pore dimensions are slightly larger than for ZSM-5 (MFI) zeolite. ZSM-12 zeolite exhibits shape selectivity and is resistant to coke formation [15,16].

Application of zeolites is not only limited to amidation of carboxylic acids, as they have been used as catalysts for amidation of alcohols [17] and ketones [18]. In the former case for example *sec*-butanol was reacting with acrylonitrile at 160 °C giving 76% selectivity to the corresponding amide with 72% conversion after 8 h [17]. Furthermore, there was an optimum Si/Al ratio observed giving the highest amide selectivity. In the latter case, in the amidation of benzophonene with hydroxylamine hydrochloride the isolated yield of amide using microwave irradiation and HY-zeolite as a catalyst of 94% was achieved in 2 min [18].

The aim in this work was to investigate the possibilities to synthesize stearoyl ethanolamide from stearic acid and ethanolamine in the absence of any volatile solvent and for the first time to use cheap supported iron catalysts in this reaction. The purpose was also to study feasibility of overall technology comprising environmentally benign methods of catalyst preparation by solid state ion exchange and reactions with inexpensive heterogeneous catalysts. The studied catalysts were characterized by several physical-chemical methods, including Mössbauer spectroscopy, gas phase pyridine adsorption desorption, liquid phase adsorption of 2-phenylethylamine, solid state NMR, nitrogen adsorption and SEM. The main parameters were the type of the support and acid sites, concentration of the latter and the oxidation state of iron.

2. Experimental

2.1. Catalyst synthesis

Several commercial zeolites and oxides were used as catalysts and supports. Silica gel 60 (Merck) was sieved with a 90 μm sieve. Titanium (IV) hydroxide granules (Alfa Aesar) were crushed and sieved with ball milling to the size below 90 μm. NH_4-Beta-300, NH_4-Beta-150, NH_4-Beta-25 and NH_4-FER-20, in which the number represents SiO_2 to Al_2O_3 ratio, were purchased from Zeolyst International and calcined in order to get the proton forms. The step calcination procedure was: heating rate of 3.8 °C/min up to 250 °C, holding at this temperature for 40 min, subsequent heating with 2.1 °C/min up to 400 °C, maintaining this temperature for 4 h, thereafter cooling zeolite to 25 °C.

To prepare iron catalysts with 5 wt% by evaporation impregnation method (EIM), 3.6 g ferric nitrate nonahydrate (Fluka) was dissolved in 250 ml of water. The pH was recorded prior and after adding 10 g of the catalyst support. The round bottom flask was put in the rotator evaporator for rotation at 60 °C during 24 h. Thereafter, water was evaporated under vacuum and the catalyst was dried at 100 °C overnight. The catalyst was then calcined in a muffle oven at a rate of 3 °C/min up to 250 °C, maintaining this temperature for 50 min, followed by heating rate of 3.3 °C/min up to 450 °C and holding this temperature for 3 h, thereafter cooling the catalyst to 25 °C. For Fe-SiO_2-50% US-EIM the slurry was first subjected to ultrasound for 2 h, followed by rotation in rotavapor for 24 h. The aqueous solution was finally evaporated, the catalyst was dried for 7 h at 100 °C and calcined in a muffle oven.

For the tin containing catalyst, the same synthesis procedure was applied with 0.905 g of tin sulfate (Fluka, ≥96%) or 1.6976 g of tin chloride (Sigma, 99%). The step calcination procedure was different from iron catalysts: initial heating rate was 2.3 °C/min up to 200 °C, maintaining this temperature for 65 min, heating to 400 °C with 2.9 °C/min, holding at 400 °C for 3 h, thereafter cooling the catalyst to 25 °C.

To prepare iron catalysts of 5 wt% by SSIE, 3.6 g of ferrite nitrate nonahydrate (Fluka) was mixed with 10 g of the catalyst support during ball milling for 6 h. Every 2 h, the equipment was stopped to manually mix and crush the solid mixture. After 6 h of ball milling, the catalyst was dried in an oven at 100 °C overnight. Then, the catalyst was calcined applying the same step calcination procedure as for iron catalysts prepared by EIM.

For the tin catalyst, the same synthesis procedure was applied with 0.905 g of tin sulfate (Fluka, ≥96%).

2.2. Catalyst characterization methods

The specific surface area was determined using nitrogen adsorption with Sorptomatic 1900. The samples were outgassed prior to measurements at 150 °C for 3 h. The specific surface areas were calculated using Dubinin's method [19,20].

XRD measurements were performed to identify the structure of zeolites using Philips X'Pert Pro MPD instrument and monochromated CuKα radiation at 40 kV/50 mA using beam collimation of 0.25° divergence slit and a fixed mask of 20 mm. Philips X'Pert HighScore and MAUD programs were used for analysis.

SEM analyses were performed with a LEO Gemini 1530 scanning electron microscope. Thermo Scientific UltraDry Silicon Detecto (SDD) was used for morphological analysis of samples. The equipment contained both secondary and backscattered electron detectors and an In-Lens detector.

The amounts of Brønsted and Lewis acid sites at bands 1545 cm^{-1} and 1455 cm^{-1}, respectively were quantified with pyridine (Sigma-Aldrich, > 99.5%) adsorption/desorption by FTIR using ATI Mattson instrument and using molar extinction coefficients from Emeis [21].

Adsorption of 2-phenylethylamine on zeolites and metal modified zeolites was investigated using 0.03 M 2-phenylethylamine as an adsorbate in distilled water [22]. Typically 50 mg of the dried catalyst was combined with 3 ml of 2-phenylethylamine (Acros Organics, 99%) solution at 24 °C. The solution was stirred with a magnet for 2 h, which was sufficient to achieve the equilibrium. The supernatant liquid after filtration of the catalyst was analyzed with UV–vis (Shimadzu UV-2550) at 252 nm. The adsorbed amounts of 2-phenylethylamine were calculated by subtracting the amount of 2-phenylethylamine present in the liquid phase from the initial adsorbent concentration. The experimental error in absorbance was 2%.

2.3. Catalyst evaluation for amidation reaction and analytical procedure

Typically the experiments were performed in an autoclave using equimolar amounts of the fatty acid (Sigma Aldrich, 95%) and ethanolamine (0.14 mol, Sigma Aldrich, > 95%) under 20 bar Ar (AGA) under high stirring speed, 1100 rpm to minimize mass transfer limitations using 0.5 g catalyst. External mass transfer was suppressed by applying small catalyst particles, below 90 μm. The liquid volume was 44 ml and the initial concentration of fatty acid was 3.0 M. The samples of reaction mixtures were silylated as follows: the solid sample was dissolved in toluene with the concentration of 1 mg/ml. Thereafter about 1 ml of the sample was silylated with 120 μl of bis(trimethylsilyl) trifluoroacetamide (BSTFA) and 0.4 μl of trimethylchlorosilane (TMCS) at 70 °C for 1 h. The samples were cooled and analyzed with a GC equipped with HP-1 column using the following temperature program: 100 °C (1.5 min) – 12 °C/min – 340 °C (20 min). The injector and

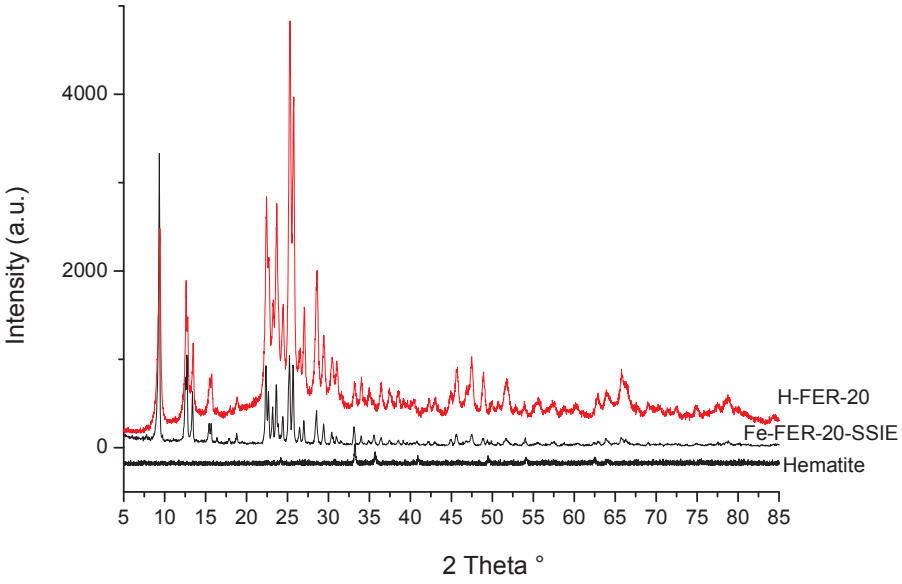

Fig. 1. Diffractogram of H-FER-20, Fe-FER-20-SSIE and Hematite (Fe_2O_3).

detector temperatures were 330 °C and 340 °C, respectively. The peaks were confirmed with GC–MS and NMR analogously to our previous publication [5].

3. Results and discussion

3.1. Catalyst characterization results

3.1.1. X-ray powder diffraction

The structure and phase purity of Fe modified Beta-25, ZSM-12-35 and Ferrierite-20 zeolite catalysts were determined using X-ray powder diffraction. The diffractogram for Fe-FER-20-SSIE is shown in Fig. 1. The corresponding diffraction patterns were similar to those of the pristine unmodified Beta (Fig. 2) [23], ZSM-12 and Ferrierite zeolites [24], indicating that Fe modification did not influence the basic structures. In order to investigate if Fe_2O_3 particles, which presence was confirmed by Mössbauer spectroscopy and discussed, are visible in XRD of Fe-FER-20-SSIE, XRD for pristine ferrierite was also made and compared with XRD of hematite [25]. The main Braggs reflection peak of hematite, 104 is found at 2Θ 33° followed by the second largest peak, 110 at 36° were also visible in Fe-FER-20-SSIE. It was, however, challenging to clearly differentiate hematite particles from ferrierite in TEM images due to low loading of iron. XRD data indicated that hematite particles in Fe-FER-20-SSIE would be larger than 3 nm.

3.1.2. Scanning electron microscopy

The morphology of the catalysts was studied using scanning electron microscopy. The SEM images of some selected catalysts are shown in Figs. 3 and 4. The shape of Fe-FER-20-SSIE crystals is rectangular, often quite long and narrow. The Fe-Beta-25-EIM crystals are circular, whereas Fe-Al_2O_3-EIM crystals have a shape of large balls with small crystal growth inside. Fe-TiO_2 crystals are very small and circular in shape, while Fe-SiO_2 crystals have sharp and thick edges.

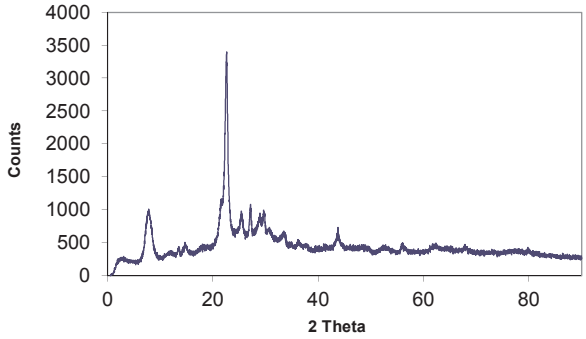

Fig. 2. X-ray powder diffraction patterns of H-Beta-25 zeolite.

3.1.3. Surface area and pore volume measurements using nitrogen physisorption

The specific surface areas of the catalysts are given in Table 1. The largest specific surface area (953 m^2/g) was measured for Fe-Beta-25-EIM zeolite catalyst, whereas Fe-TiO_2-SSIE exhibited the lowest specific surface area (90 m^2/g). The reason for a very large surface area for Fe-Beta-25-EIM zeolite catalyst is attributed to the presence of a large amount of micropores. In addition Fe-FER-20-SSIE zeolite catalyst exhibited even a lower specific surface area (384 m^2/g), which was 17% lower than the specific surface area (464 m^2/g) of pristine H-FER. Fe-H-ZSM-12-35-EIM catalyst displayed also a low specific surface area.

3.1.4. Determination of acidity

Acidity of the catalysts was elucidated by pyridine adsorption-desorption from the gas phase and via adsorption of phenyl ethylamine from distilled water. The results from pyridine adsorption-desorption showed that Fe-SiO_2 exhibited a very low acidity as expected. Fe-TiO_2–SSIE showed only Lewis acidity. Fe-ZSM-12-35-EIM displayed very low acidity according to pyridine FTIR. Due to its small pore sizes, it can be, however, concluded that pyridine is not capable to enter the pores of ZSM-12 giving thus very low acidity values reflecting only the external surface. The Brønsted acidity of H-FER was the highest one featuring also large amounts of strong acid sites (Table 1). When Fe was loaded on H-FER, the concentration of Brønsted acid sites of the resulting Fe-H-FER-20-SSIE was only 54% of H-FER initial acidity. The amount of Brønsted acid sites in Fe-Beta-25-EIM catalyst was 13% higher than that of H-Beta-150-SSIE as expected. Noteworthy is, however, that the amount of strong acid sites increased in the following order: Fe-Beta-25-EIM > Fe-Beta-150-SSIE > Fe-FER-20-SSIE. When comparing the acidity values measured with pyridine adsorption desorption to that of amine adsorption (Fig. 5), it can be seen that Fe-Beta-25-EIM exhibited high acidity according to both methods. Unexpectedly, the amine adsorption capacity of Fe-Beta-150-EIM was higher than that of Fe-Beta-25-EIM (Fig. 5), although they have almost the same total capacity for adsorption of pyridine. The latter catalyst contains also more Brønsted acid sites than the former one. On the other hand, acidity of especially H-FER measured by amine adsorption was lower than determined by pyridine adsorption-desorption method. Iron

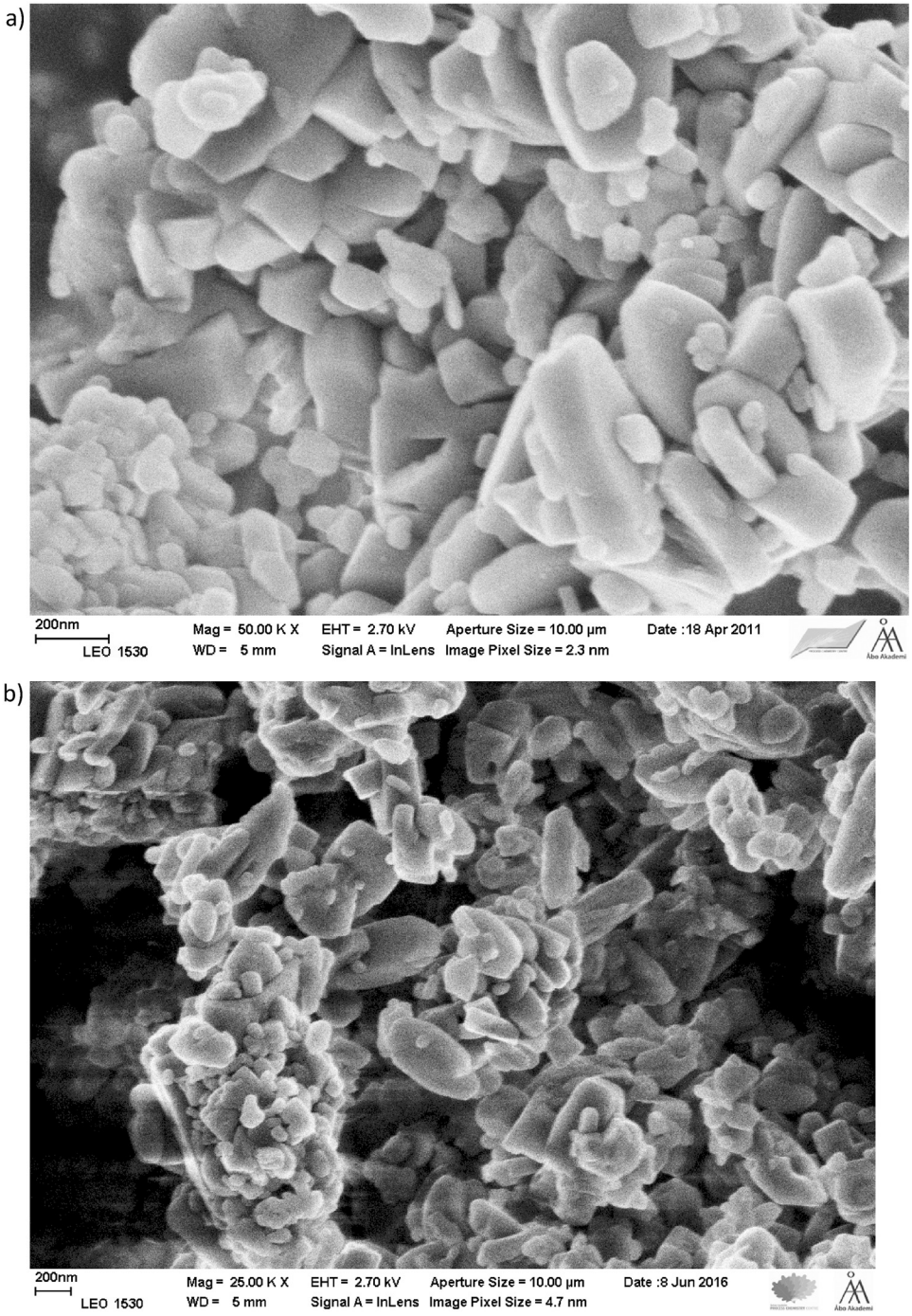

Fig. 3. Scanning electron micrographs of (a) 1.8 wt% Fe-FER-20-SSIE and (b) H-FER-20.

loaded Fe-FER-20-SSIE exhibited a rather low acid site concentration based on amine adsorption. These results can be correlated with the fact that 2-phenylethylamine is a rather large molecule having difficulties in penetrating into the pores of FER. Noteworthy is the acidity measured for Fe-TiO_2-SSIE, which was relatively large based on 2-phenylaethylamine adsorption in comparison to pyridine adsorption-desorption. Both methods indicated very low acidity of Fe-ZSM-12-35-EIM reflecting difficulties of adsorbate penetration into narrow pores of this material.

^{27}Al NMR showed clearly that tetrahedrally and octahedrally coordinated Al species at 55 ppm and close to zero ppm were clearly visible in the spectra [27]. The ratio between tetrahedrally to octahedrally coordinated Al-species decreased in the following order: Fe-H-Beta-25-EIM ~ Fe-ZSM-12-35-EIM > > > Fe-H-Beta-150-SSIE (Table 2), which is in line with the pyridine adsorption-desorption results. As mentioned above acidity of ZSM-12 is related to its pore size.

3.1.5. Measurement of the oxidation states of Fe using Mössbauer spectroscopy

The Mössbauer spectra of Fe-H-FER-SSIE, Fe-H-Beta-25-EIM and Fe-Al_2O_3-EIM catalysts are given in Fig. 6a–c. The oxidation states of Fe i.e. FeO, α-Fe_2O_3, Fe_3O_4 and Fe^0 studied in the above catalysts showed the presence of magnetic, paramagnetic and super magnetic oxides. 1.8 wt % Fe-Ferrierite-20-SSIE, the most active and selective catalyst in amidation of stearic acid, exhibited two paramagnetic compounds with isomer shifts of 0.20 mm/s and 0.21 mm/s attributed to Fe (III). Fe-FER-20-SSIE sample contained also large amounts of magnetic iron oxides which was probably hematite, Fe_2O_3, about 60% and the two

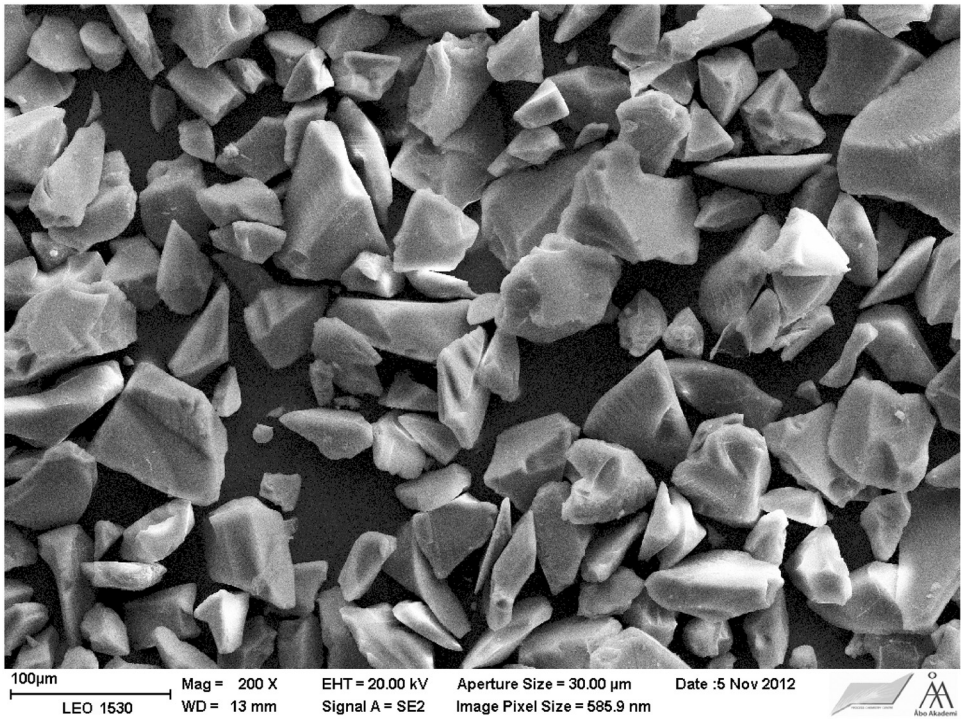

Fig. 4. Scanning electron micrograph of Fe-SiO_2 US-50%-EIM catalyst.

other iron species with oxidation state of III which were paramagnetic. The influence of Fe content on the oxidation states of Fe in Ferrierite zeolite was previously studied using Mössbauer spectroscopy [28] showing that the amount of Fe in Ferrierite influenced the oxidation states. Isomer shifts for Fe (II) and Fe (III) were reported to be dependent on the amount of Fe present in Ferrierite, in the study where the iron loading was very low, below 0.3the molar ratio of Fe/Al [29].

4.8 wt% Fe-H-Beta-25-EIM zeolite prepared by the evaporation impregnation method showed two paramagnetic compounds with isomer shifts < 0.5 mm/s both tentatively attributed to Fe (III) at 0.4 mm/s, with one component being slightly shifted towards divalency (isomer shift 0.40 mm/s). It is also noteworthy to mention, that isomer shifts of Fe were observed to be influenced by the type of structures for Beta (BEA), Ferrierite (FER) and ZSM-5 (MFI) zeolites [29].

For 3.8 wt% Fe-Al_2O_3–EIM catalyst prepared using evaporation-impregnation method, three paramagnetic compounds with isomer shifts obtained were at 0.44 mm/s, 3.0 mm/s and 0.13 mm/s. The compound with a negative isomer shift could be due to the presence of Fe(IV). Analogously to 4.8 wt% Fe-H-Beta-25-EIM, all iron was also paramagnetic in 3.8 wt% Fe-Al_2O_3–EIM. Hence, based on the Mössbauer spectra results of the studied catalysts, Fe isomer shifts were influenced by the amount of Fe, structure and acidity of the catalysts.

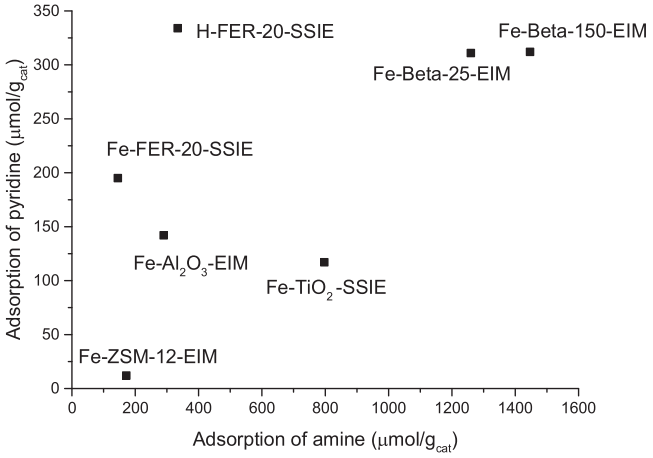

Fig. 5. Acid site concentration from pyridine adsorption-desorption with gas phase versus 2-phenylethylamine adsorption from aqueous phase.

Furthermore, catalytic activity and selectivity in stearic acid amidation were also observed to be correlated with the isomer shifts of the studied catalysts, and thus with the presence of different iron species.

Table 1
Brønsted and Lewis acidity of selected used catalysts.

Catalyst	Specific surface area (m^2/g_{cat})	Pore volume (cm^3/g_{cat})	Brønsted acid sites (µmol/g_{cat})			Lewis acid sites (µmol/g_{cat})			Refs.
			250 °C	350 °C	450 °C	250 °C	350 °C	450 °C	
4.6 wt% Fe-SiO_2-50% US-EIM	389	0.68	4	4	2	5	3	1	[26]
3.8 wt% Fe-Al_2O_3-EIM	261	1.13	12	12	6	140	62	12	[26]
4.5 wt% Fe-TiO_2-SSIE	90	0.27	0	0	0	117	0	0	This work
6.4 wt% Fe-ZSM-12-35-EIM	109	0.04	0	0	0	12	0	0	This work
5.3 wt% Fe-Beta-150-SSIE	467	0.59	193	137	45	119	41	4	[26]
4.8 wt% Fe-Beta-25-EIM	953	0.65	216	168	17	95	36	5	This work
1.8 wt% Fe-Fer-20-SSIE	384		176	169	74	19	15	4	[24]
4.3 wt% Sn-FER-20-EIM	949								
H-FER-20	464		326	284	170	8	7	4	[24]

Table 2
Results from ^{27}Al MAS NMR for different Fe-modified zeolites.

Catalyst	Al(tetrahedral) (ppm)	Al(octahedral) (ppm)	Al(tetrahedral) /Al(octahedral)
5.3 wt% Fe-Beta-150-SSIE	53.74	−0.64	4.0 ± 0.1
4.8 wt% Fe-H-Beta-25-EIM	54.46	−0.65	9.0
6.4 wt% Fe-ZSM-12-35-EIM	51 ± 1	−0 ± 1	25

3.2. Catalytic evaluation of stearic acid amidation

3.2.1. Thermal amidation of stearic acid

Thermal amidation of stearic acid with an equimolar amount of ethanolamine proceeded at 180 °C in an autoclave very rapidly in the absence of any solvent giving 90% conversion within 1 h (Table 3). This is much higher conversion than achieved at the same temperature in hexane as a solvent, when conversion of stearic acid of only 61% after 5 h was reported [6]. Thus it can be concluded that a higher reaction rate is related to a higher initial stearic acid concentration. High activity of undiluted stearic acid was supported by experimental data at 160 °C giving conversion 73% after 1 h. An important question is related to a potential impact of reactor walls and impeller material made of stainless steel as they could also act as a catalyst in addition to the

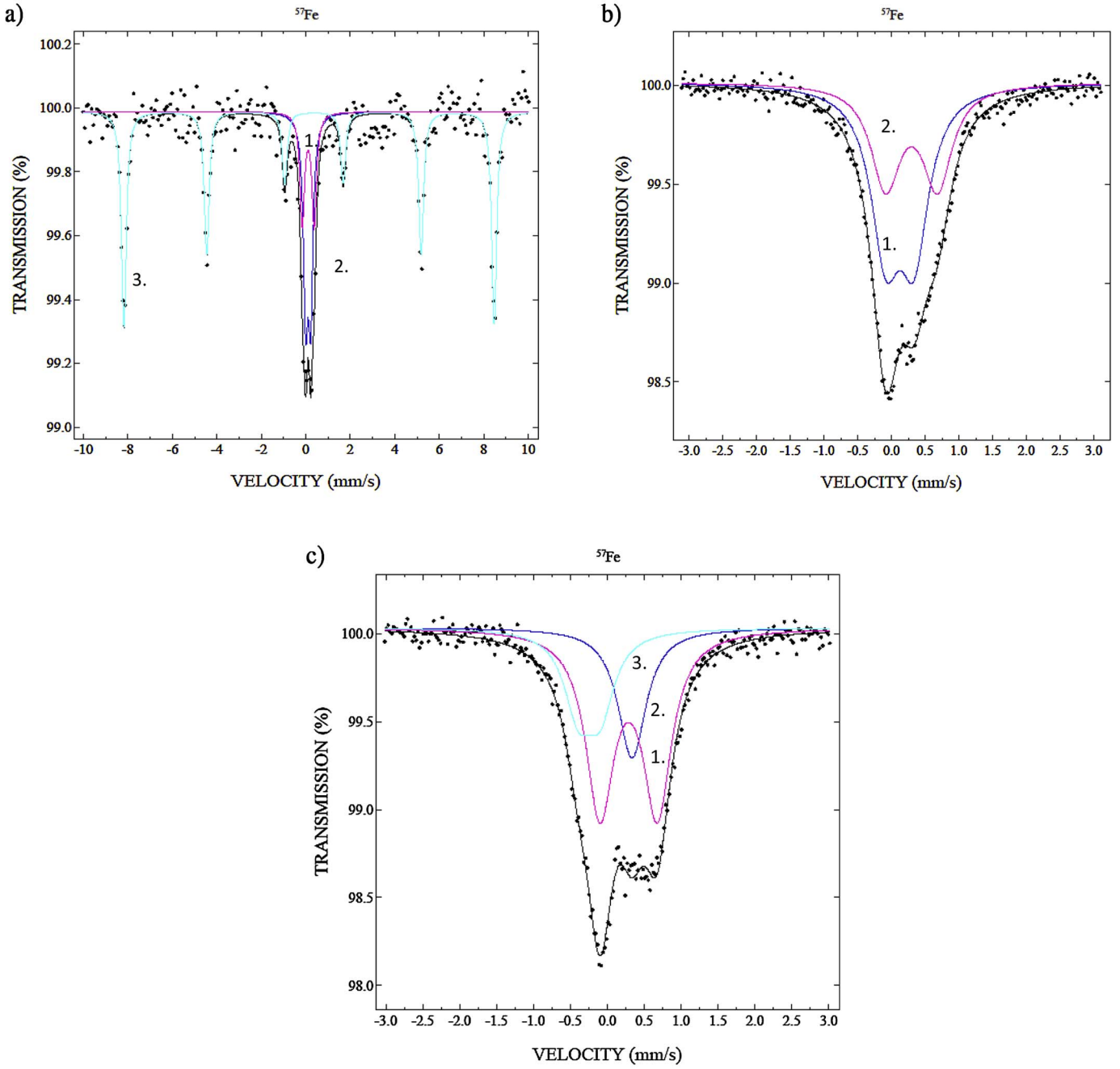

Fig. 6. Mössbauer spectra (a) 1.8 wt% Fe-H-FER-20-SSIE zeolite catalyst, notation: 1. line corresponds to magnetic hematite, 2. and 3. lines correspond to paramagnetic trivalent Fe_2O_3, (b) 4.8 wt% Fe-Beta-25-EIM zeolite catalyst, notation: the sample is fully paramagnetic, 1. line corresponds to trivalent iron, 2. line is most probably trivalent, but slightly shifted towards Fe^{2+} and (c) 3.8 wt% Fe-Al_2O_3-EIM catalyst, notation: all iron paramagnetic, 1. line trivalent iron, 2. line, trivalent, 20.3%, 3. line, corresponds possibly to tetravalent, 23.4%.

Table 3
Results from the amidation of stearic acid with an equimolar amount of ethanolamine in a batch reactor.

Entry	Catalyst	Temperature (°C)	Mass of catalyst (g)	Time (h)	Conversion (%)	Mole converted SA per mol Fe	Selectivity to amide (mol-%)	Selectivity to esteramide (mol-%)
1	No	180	–	1	90	–	92	0
2	No	160	–	1	73	–	95	0
3	No	140	–	1	7			
4	No	140	–	5	78	–	97	
5	No	120	–	1	4	–	100	0
6	No	120	–	5	15	–	95	0
7	Fe_2O_3	120	2	1	17	2	95	0
8	3.8 wt% Fe-Al_2O_3-EIM	120	0.5	5	26	104	90	3
9	Al_2O_3	120	0.5	5	17	–	–	0
10	4.6 wt% Fe-SiO_2-50% US-EIM	120	0.5	1	22	72	96	4
11	4.6 wt% Fe-SiO_2-50% US-EIM	120	0.5	5	32	106	97	0
12	4.5 wt% Fe-TiO_2-SSIE	120	0.5	5	11	37	93	0
13	6.4 wt% Fe-ZSM-12-35-EIM	120	0.5	1	32	75	94	0
14	6.4 wt% Fe-ZSM-12-35-EIM	120	0.5	5	32	76	97	3
15	4.6 wt% Fe-SiO_2 and H-6.4 wt% ZSM-12-35-EIM	120	0.5	5	29	95	100	0
16	1.8 wt% Fe-FER-20-SSIE	120	0.5	1	26	219	97	0
17	1.8 wt% Fe-FER-20-SSIE	140	0.5	1	61	538	98	2
18	1.8 wt% Fe-FER-20-SSIE	120	0.5	5	33	277	100	0
19	Sn-FER-20-EIM	120	0.5	5	10	30[a]	93	0
20	H-FER-20	120	0.5	5	23	–	89	0
21	4.8 wt% Fe-Beta-25-EIM	120	0.5	5	25	81	97	0
22	5.3 wt% Fe-Beta-150-SSIE	120	0.5	5	22	109	90	4
23	no[b]	120	–	5	12	–	93	0
24	5.3 wt% Fe-Beta − 150-SSIE[b]	120	0.5	5	4	42	71	0

[a] Calculated per mole of Sn.
[b] Reactive distillation with stepwise addition of ethanolamine, 0.8 g per batch, corresponding to the molar ratio of SA:EA (stearic acid = SA, ethanol amine = EA) of 1:1 in each 30 min.

thermal reaction. A decrease of the reaction temperature resulted in non-negligible conversions of stearic acid equal to 7% and 4%, respectively at 140 °C and 120 °C. The subsequent step was to investigate the catalytic effect of iron.

3.2.2. Iron catalyzed amidation of stearic acid

To investigate the effect of bulk iron, 2 g of Fe_2O_3 was used as a catalyst for 0.31 mol of stearic acid with an equimolar amount of ethanolamine at 120 °C. The result showed that even bulk iron oxide has a catalytic effect, since the conversion after 1 h was 17% (Table 3), being in the absence of any catalyst only 4%.

A systematic catalyst screening study for amidation of stearic acid was performed at 120 °C, since under these conditions noncatalytic stearic acid conversion was only 4% and 15% after 1 and 5 h, respectively. When the supported iron catalyst (Fe-Al_2O_3-EIM) was used, the conversion after 5 h was 26% showing clearly that it acts more efficiently as a catalyst than plain hematite. In addition, catalyst productivity, calculated as the moles of converted stearic acid per mole of iron was much higher for Fe-Al_2O_3-EIM compared to hematite (Table 3). When only Al_2O_3 was used, conversion of 17% was achieved in 5 h also reflecting the catalytic effect of iron.

To avoid interference of sampling the solvent-free amidation of stearic acid with an equimolar amount of ethanolamine was conducted by analyzing only the final mixtures for experiments lasting either 1 or 5 h. The results revealed that conversion of stearic acid increased with 4.6 wt% Fe-SiO_2-EIM and 1.8 wt% Fe-FER-20-SSIE when the reaction time was prolonged from 1 h to 5 h (Fig. 7). On the other hand, with the medium pore size zeolite, ZSM-12-35-EIM the same conversion levels were obtained after 1 and 5 h indicating strong deactivation which can be explained by its small pore size compared to the size of the reactants and products leading to pore blockage. The conversion levels, however, remained in the range of 32 − 33% after 5 h experiment for 4.6 wt% Fe-SiO_2-50% US-EIM, 6.4 wt% Fe-ZSM-12-35-EIM and 1.8 wt% Fe-FER-SSIE-20. In order to check if these conversion levels correspond to the equilibrium, the latter were determined for amidation of stearic acid

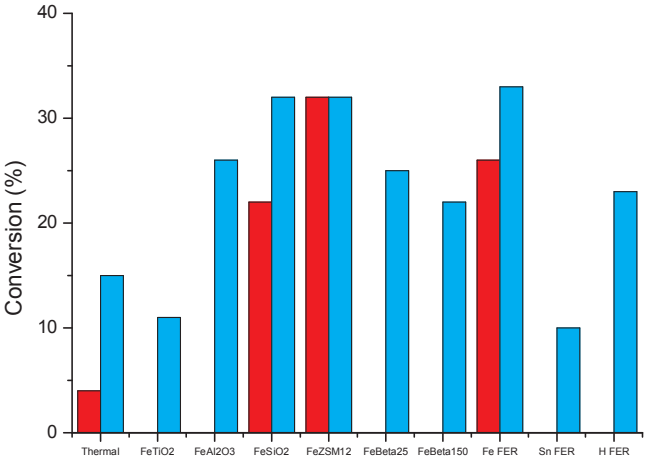

Fig. 7. Conversion of stearic acid in its amidation with an equimolar amount of ethanolamine at 120 °C after 1 h (red bar) or 5 h (blue bar) using 0.5 g of different catalyst. In comparison results from thermal amidation are given. (For interpretation of the references to colour in this figure legend, the reader is referred to the web version of this article.)

using the Gibbs free energy at 120 °C, calculated with HyperChem programme [7]. ΔG_{393K} was equal to −0.1 kJ/(K mol) giving the equilibrium conversion of 50% showing that the experimental conversion was lower than corresponding to the equilibrium one.

In order to compare catalytic activity in terms of turnover frequencies (TOF) of different catalysts, the particle sizes of different iron species, for example hematite, should be determined. While XRD results indicate presence of hematite particles larger than 3 nm, it is, however, difficult to approximate the sizes due to partially overlapping peaks in pristine Ferrierite. Iron particle sizes could be determined by CO chemisorption at −78 °C [30], which is not feasible with the setup used in this work. Moreover, in the current case the catalyst was not reduced prior to the reaction, as done for example in Fischer-Tropsch synthesis,

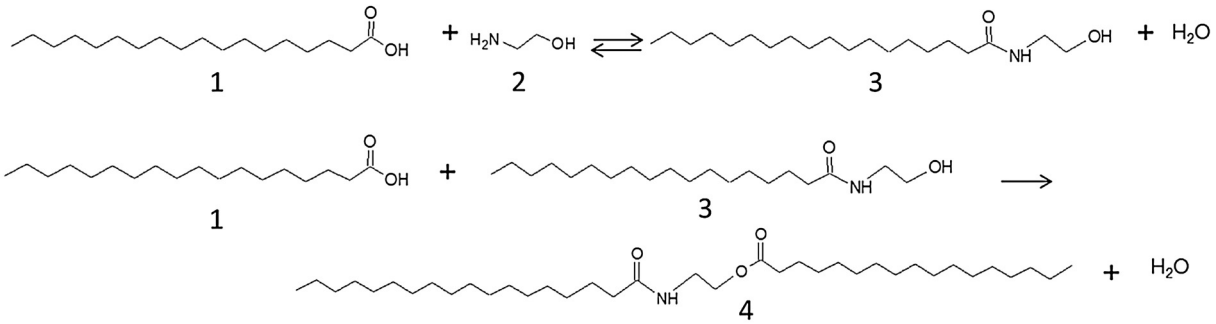

Scheme 1. Reaction scheme for stearic acid (1) amidation with ethanolamine (2). Notation: stearylethanolamide (3) and esteramide (4).

allowing correlation of hydrogen uptake with catalytic activity [31]. Due to such specific features of iron containing catalyst, the catalytic activity is typically correlated only with the oxidation state of iron as for example in benzene oxidation to phenol [32].

When the batch operation mode was used, the formed water was accumulating in the reactor, shifting the reaction towards the reactants (Scheme 1). Thus some experiments were also performed under atmospheric pressure using a reactive distillation option, when water can be evaporated continuously from the reactor while ethanolamine was added in several batches. Acceptable levels of ethanolamine vapor pressure at 120 °C permitted injection of ethanolamine into the stearic acid melt containing the catalyst. The conversion remained, however, at a quite low level, most probably due to high viscosity of the reaction mixture retarding water evaporation.

The effect of specific surface area on iron dispersion and subsequently on stearic acid reactivity in amidation was clearly visible, for example with oxide supported Fe-catalysts. The lowest conversion among Fe-oxide catalysts was achieved with Fe-TiO_2–SSIE exhibiting the lowest specific surface area of 90 m^2/g_{cat} followed by Fe-Al_2O_3-EIM and Fe-SiO_2-EIM. Fe-FER-20-SSIE, which also gave a relatively high conversion of stearic acid, possesses a high specific surface area. It should, however, be stated that due to strong acidity of some zeolites, with high specific surface area and high dispersion of iron, e.g. Fe-Beta-150-SSIE, catalyst deactivation is prominent. When comparing the performance of different catalysts in terms of productivity (moles of converted stearic acid per moles of iron), Fe-FER-20-SSIE is much better than Fe-SiO_2-50% US-EIM and Fe-ZSM-12-35-EIM, with the corresponding ratios being 277, 106 and 76, respectively. In addition, bearing in mind that for both Fe-FER-20-SSIE and Fe-ZSM-12-35-EIM all iron and acidic sites are not accessible, the result is even more apparent indicating that Fe-FER-20-SSIE is the best catalyst among tested due to its optimum acidity.

The effect of the type, strength and concentrations of acid sites in the studied catalysts on stearic acid amidation can be seen in Figs. 8 and 9. The results showed that the highest conversion was obtained with Fe-ZSM-12-35, Fe-SiO_2–EIM and Fe-FER-20-SSIE, which exhibit different acidities. The acid sites in Fe-ZSM-12-35-EIM are most probably not accessible for the reactants due to too small pores of the zeolite. Fe-SiO_2–EIM exhibits only very low acidity, being still active in stearic acid amidation. Fe-FER-20-SSIE with a relatively high acidity and especially a high amount of strong acid sites seems to be beneficial for the reaction. Noteworthy is that Fe-Beta-25-EIM with relatively large pores, but only a small amount of strong acid sites, gave conversion lower than Fe-FER-20-SSIE. This result indicates that also presence of strong Brønsted acid sites is beneficial for amidation. On the other hand, when only H-FER was used as a catalyst, conversion of stearic acid was low, H-FER exhibited nearly two fold strong acid sites compared to Fe-FER-SSIE-20. It should also be noted that Sn-FER-20-EIM did not have any catalytic effect, moreover, conversion with this material was even lower than thermal amidation per se. The effect of the ratio between Brønsted to Lewis acid site concentration on stearic acid conversion is also visible in

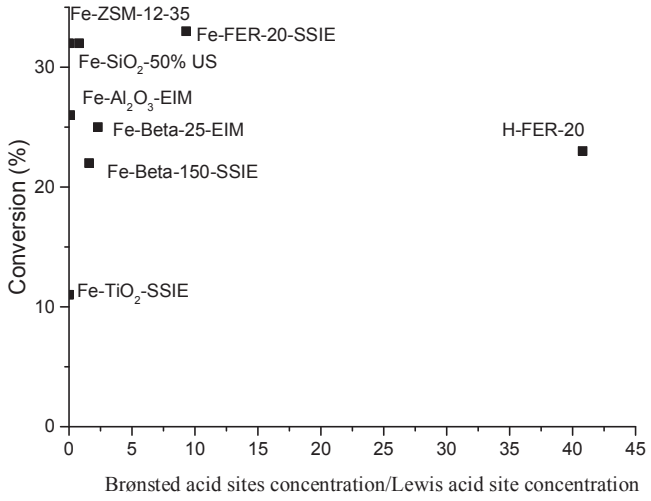

Fig. 8. Conversion of stearic acid in its amidation with an equimolar amount of ethanolamine at 120 °C after 5 h using 0.5 g of different catalysts as a function of the ratio of Brønsted to Lewis acid site concentrations.

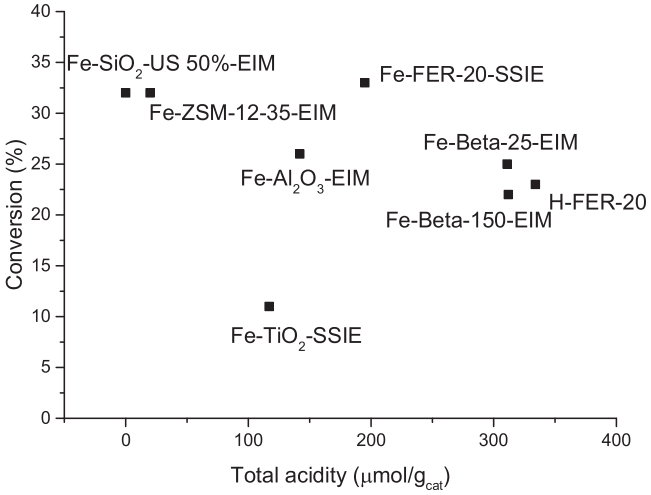

Fig. 9. Conversion of stearic acid in its amidation with an equimolar amount of ethanolamine at 120 °C after 5 h using 0.5 g of different catalyst as a function of the sum of Brønsted and Lewis acidity of the catalyst (measured by pyridine adsorption).

Fig. 8. It can be clearly seen that conversion was the lowest with the catalysts having only Lewis acidity, such as Fe-TiO_2-SSIE, exhibiting low specific surface area. A relatively high conversion was achieved with mildly acidic Fe-SiO_2-50% US-EIM with a large specific surface area. When the ratio between Brønsted to Lewis sites increased, the conversion of stearic acid increased. A high conversion was also achieved with Fe-FER-20-SSIE. H-FER exhibited too high concentration of Brønsted acid sites leading to catalyst deactivation. These results

indicate that too high amount of strong Brønsted acid sites is not favorable for the amidation of stearic acid or alternatively that Fe is highly dispersed on a non-acidic catalyst. Selectivity to amide was always very high and only a limited amount of esteramide was formed.

From the above mentioned results, it can be concluded that supported iron catalysts have a clear catalytic effect in stearic acid amidation with an equimolar amount of ethanolamine in the absence of any solvent. High iron dispersion is beneficial for stearic acid amidation. An optimum amount of strong Brønsted acid sites in addition to high Fe dispersion is also required for catalyst efficiency. For the catalyst most active at 120 °C, Fe-FER-20-SSIE, amidation of stearic acid was also performed at 140 °C. A blank experiment in the absence of any catalyst was also conducted. The results revealed that the non-catalyzed amidation at 140 °C gave only 7% conversion after 1 h of reaction time, whereas with Fe-FER-20-SSIE the conversion was 61%. In addition to a relatively low concentration of Brønsted acid sites, this catalyst contained mostly iron as Fe^{3+} species which are apparently promoting amidation of stearic acid. This result is very promising showing clearly that a bifunctional Fe-modified zeolite is active and selective catalyst for production of stearoyl ethanolamide in the absence of any solvent.

4. Conclusions

Solvent-free amidation of stearic acid with ethanolamine for production of surfactants and pharmaceuticals was investigated for the first time using inexpensive iron-supported catalysts.

Iron-modified SiO_2, Al_2O_3, TiO_2 as well as Fe containing Ferrierite, ZSM-12 and Beta zeolite catalysts were synthesized using solid state ion-exchange and evaporation impregnation methods. Structural integrity of the Fe modified catalysts studied with X-ray powder diffraction and scanning electron microscopy showed that the parent structures of the support were kept intact. Mössbauer spectroscopy of the most active and selective catalyst in the amidation of stearic acid, 1.8 wt% Fe-Ferrierite-20-SSIE exhibited the presence of Fe (III) species. 4.8 wt% Fe-Beta-25-EIM contained Fe (II) and Fe (III), whereas iron in mildly acidic Fe-Al_2O_3-EIM was present as magnetite with Fe (IV) and hematite containing Fe (III), respectively.

The most active and selective catalyst for amidation of stearic acid with ethanolamine was 1.8 wt% Fe-Ferrierite-20-SSIE containing mainly Fe^{3+} species and an optimum concentration of acid sites, especially a low amount of Brønsted acid sites. The highest conversion (61%) of stearic acid and selectivity (98%) to amide at 140 °C in 1 h was obtained over this catalyst, which was superior to other catalysts in terms of catalyst productivity per mole of iron. In addition, a nonacidic Fe-SiO_2 with large pores and slightly higher iron loading gave also high conversion. Noteworthy was also that Fe-ZSM-12-35-EIM with a smaller pore size facilitated high conversion of stearic acid despite accessibility of only external surface.

These results indicated that although there are several parameters influencing selectivity in amidation of stearic acid and further studies are needed to fully optimize the catalyst properties, application of supported iron catalysts in solvent-free conditions is a promising and an environmentally benign route to produce fatty alkanolamides.

References

[1] L. Hamtiaux, J. Masquelier, G.G. Muccioli, C. Bouzin, O. Feron, B. Gallez, D.M. Lambert, BMC Cancer 12 92 (2012) 1–14.
[2] R. Romani, R. Galezzi, G. Rosi, R. Fiorini, I. Pirisinu, A. Ambrosini, G. Zolese, Biochimie 93 (2011) 1584–1591.
[3] S. Chaudhari, J. MacDougall, J. Peters, J. Ramsbottom, Preparation of amino acid fatty acid amides, US patent 2008/0200704 A1.
[4] Y.F. Suen, S.L. Jensen, Method for preparing mono or dialkanol amides, WO2013154689, 2013, Chevron Oronite Company LLC
[5] A. Tkacheva, I. Dosmagambetova, Y. Chapellier, P. Mäki-Arvela, I. Hachemi, R. Savela, R. Leino, C. Viegas, N. Kumar, K. Eränen, J. Hemming, A. Smeds, D. Yu Murzin, ChemSusChem 8 (2015) 2670–2680.
[6] P. Mäki-Arvela, A. Tkacheva, I. Dosmagambetova, Y. Chapelliere, I. Hachemi, N. Kumar, A. Aho, D. Yu Murzin, Top. Catal. 59 (2016) 1151–1164.
[7] P. Mäki-Arvela, N. Kumar, Y. Chapelliere, I.L. Simakova, D. Yu. Murzin, React. Kinet. Mech. Catal. 120 (2017) 15–29.
[8] M. Musteata, V. Musteata, A. Dinu, M. Florea, V.T. Hoang, D. Trong-On, S. Kaliaguine, V.I. Parvulescu, Pure Appl. Chem. 79 (2007) 2059–2068.
[9] B. Sheedhar, V. Bhaskar, Ch. Sridkar, T. Srinivas, L. Kotai, K. Szenthályi, J. Mol. Catal. A: Chem. 191 (2003) 141–147.
[10] K.V.V. Krishna Mohan, N. Narender, S.J. Kulkarni, Green Chem. 6 (2006) 368–372.
[11] S. Ghosh, A. Bhaumik, J. Mondal, A. Mallik, S. Sengupta (Bandyopadhyay), C. Mukhopahahya, Green Chem. 14 (2012) 3220–3229.
[12] R. Gava, A. Biffis, C. Turbaro, F. Zaccheria, N. Ravasio, Catal. Commun. 40 (2013) 63–65.
[13] R. Fu, Y. Yang, W. Feng, Q. Ge, Y. Feng, X. Zeng, W. Chai, J. Yi, R. Yuan, Tetrahedron 72 (2016) 8319–8326.
[14] M. Mirza-Aghayan, M.M. Tavana, R. Boukherroub, Ultrason. Sonochem. 29 (2016) 371–379.
[15] R.B. La Pierre, A.C. Rohrman Jr., J.L. Schlenker, J.D. Wood, M.K. Rubin, W.J. Rohrbaugh, Zeolite 5 (1985) 346–348.
[16] X. Wei, Ps G. Smirniotis, Microporous Mesoporous Mater. 97 (2006) 97–106.
[17] K.V.N.S. Srinivas, E. Bolla Reddy, B. Das, SynLett 4 (2002) 625–627.
[18] S.-C. Wu, J.S.B. Wang, T.-C. Tsai, Top. Catal. 53 (2010) 1419–1429.
[19] M.M. Dubinin, Carbon 27 (1989) 457–467.
[20] S.G. Chen, R.T. Yang, Langmuir 10 (1994) 4244–4249.
[21] C.A. Emeis, J. Catal. 141 (1993) 347–354.
[22] V. Rac, V. Rakic, D. Stosic, O. Otman, A. Auroux, Microporous Mesoporous Mater. 194 (2014) 126–134.
[23] W. Guo, C. Xiong, L. Huang, Q. Li, J. Mater. Chem. 11 (2001) 1886–1890.
[24] N. Kumar, P. Mäki-Arvela, S. Faten Diaz, A. Aho, Y. Demidova, J. Linden, A. Shepidchenko, M. Tenhu, J. Salonen, P. Laukkanen, A. Lashkul, J. Dahl, I. Sinev, A.-R. Leino, K. Kordas, T. Salmi, D. Yu Murzin, Top. Catal. 56 (2013) 696–713.
[25] D. Peng, S. Beysen, Q. Li, Y. Sun, L. Yang, Particuology 8 (2010) 386–389.
[26] M. Stekrova, N. Kumar, A. Aho, I. Sinev, W. Grunert, J. Dahl, J. Roine, S. Arzumanov, P. Mäki-Arvela, D. Yu Murzin, Appl. Catal. A. Gen. 470 (2014) 162–176.
[27] P.P. Pescarmona, K.P.F. Janssen, C. Strobants, B. Molle, J.S. Paul, P.A. Jacobs, B.F. Sels, Top. Catal. 53 (2010) 77–85.
[28] E. Tabor, K. Zavet, N.K. Sathu, Z. Tvaruzkova, Z. Sobalik, Catal. Today 169 (2011) 16–23.
[29] K. Jisa, J. Novakova, M. Schwarze, A. Vondrova, S. Sklenak, Z. Sobalik, J. Catal. 262 (2009) 27–34.
[30] P.H. Emmett, S. Brunauer, J. Am. Chem. Soc. 59 (1937) 310–315.
[31] C.-H. Zhang, Y. Yang, B.-T. Teng, T.-Z. Li, H.-Y. Zheng, H.-W. Xiang, Y.-W. Li, J. Catal. 237 (2006) 405–415.
[32] E. Hensen, Q. Zhu, P.-H. Liu, K.J. Chao, R. van Santen, J. Catal. 226 (2004) 466–470.